RSC Applied Interfaces

ROYAL SOCIETY OF CHEMISTRY

PAPER

View Article Online
View Journal | View Issue

Cite this: *RSC Appl. Interfaces*, 2025, **2**, 1345

Optimizing ZIF-8 membrane growth on top of semiconductive Ga-doped ZnO sensitive layers†

Kevin Dedecker, *[a] Benjamin Paret,[b] Lionel Presmanes,*[b] Benjamin Duployer,[b] Antoine Barnabé, [b] Philippe Menini, [c] David Farrusseng, [d] Mikhael Bechelany, [ae] Martin Drobek *[a] and Anne Julbe [a]

Received 25th February 2025,
Accepted 9th June 2025

DOI: 10.1039/d5lf00054h

rsc.li/RSCApplInter

Functionalizing ZnO-based chemiresistive sensor surfaces with a ZIF-8 layer, which acts as a permselective membrane, is a well-established strategy to enhance sensor selectivity. This study examines the key factors influencing the conversion process, including the physicochemical properties of solvents or solvent mixtures and the thermal pretreatment, of Ga-doped ZnO (ZnO : Ga). We have evidenced that the polarity, viscosity, and interfacial tension of the solvent significantly affect the dissolution of ZnO : Ga and the crystallization of ZIF-8. Methanol–water mixtures were found to effectively control the conversion process, with a 3 : 1 MeOH/H_2O ratio being optimal for producing continuous ZIF-8 membranes. Additionally, it has been demonstrated that annealing can greatly enhance the reactivity of the oxide. However, while it enhances the dissolution of ZnO : Ga, excessively high temperatures can lead to over-dissolution, which hinders ZIF-8 formation. These insights are crucial for optimizing ZIF-8 layers on ZnO : Ga, paving the way for the development of highly selective chemiresistive sensors.

Introduction

Metal oxide (MO_x) chemiresistive sensors,[1,2] such as those based on SnO_2, WO_3, In_2O_3, and ZnO, are widely used for detecting gases and VOCs in industrial and domestic settings. They are valued for their low cost, portability, ease of use, real-time and very long-term monitoring capabilities. With sensitivity reaching levels below parts per billion, these devices often outperform traditional technologies like electrochemical sensors. Detection relies on redox reactions between MO_x and target molecules, altering the electrical resistance.[3] The performance of those sensors is mainly influenced by factors such as MO_x layer thickness, grain boundaries, operating temperature, and doping levels.

Zinc oxide (ZnO) is a key material for gas sensors due to its non-toxicity, low cost, and high electron mobility. As an n-type semiconductor with a wide bandgap (3.37 eV) and excellent carrier mobility,[4–6] ZnO shows great potential for sensing applications. However, its high resistivity often limits the sensing performance.[7] To overcome this limitation, doping with gallium (Ga) effectively reduces resistivity, enhances oxidation resistance, and improves thermal stability.[8–10] Ga-doped ZnO (ZnO : Ga) is therefore considered as one of the most promising materials for fabricating sensitive sensors,[11] as demonstrated by Presmanes and coworkers in their sub-ppm NO_2 sensing studies.[12] Despite these advances, ZnO : Ga sensors, like their other MO_x counterparts, continue to face challenges with selectivity, especially in the presence of interfering molecules. This necessitates further optimization for practical sensing applications.

To address the issue of limited selectivity in chemiresistive sensors, a promising solution involves applying a selective membrane as an overlayer on the MO_x-based sensing material. This strategy has proven effective in various systems, including nanowire-based sensors like SnO_2 coated with Al_2O_3 (SnO_2@Al_2O_3)[13] and ZnO combined with boron nitride and palladium (ZnO@boron nitride/Pd).[14] These selective membranes not only enhance the selectivity of the

[a] *Institut Européen des Membranes (IEM-UMR 5635) CNRS, ENSCM, Univ Montpellier, Place Eugène Bataillon, 34095 Montpellier Cedex 5, France. E-mail: kevin.dedecker@umontpellier.fr, martin.drobek@umontpellier.fr*
[b] *Centre Interuniversitaire de Recherche et d'Ingénierie des Matériaux (CIRIMAT-UMR 5085), Université de Toulouse, Université Toulouse 3 Paul Sabatier, Toulouse INP, CNRS, 118 Route de Narbonne, Cedex 9, 31062 Toulouse, France. E-mail: lionel.presmanes@univ-tlse3.fr*
[c] *Laboratoire d'Analyse et d'Architecture des Systèmes (LAAS-UPR 8001), Université de Toulouse, CNRS, UPS, 7 Avenue du Colonel Roche, Cedex 4, 31031 Toulouse, France*
[d] *Institut de recherches sur la catalyse et l'environnement de Lyon (IRCELYON-UMR 5256), Université de Lyon, CNRS, 2 Avenue Albert Einstein, 69626 Villeurbanne Cedex, France*
[e] *Functional Materials Group, Gulf University for Science and Technology, Mubarak Al-Abdullah, 32093, Kuwait*

† Electronic supplementary information (ESI) available: Additional material characterizations and computational details. See DOI: https://doi.org/10.1039/d5lf00054h

sensors but also improve their stability and reliability in complex environments. It is worth noting that metal–organic frameworks (MOFs) have also been studied as membrane overlayers to enhance the selectivity of chemiresistive sensors[15,16] forming interfaces conceptually similar to heterojunctions observed in certain metal-oxide clusters.[17]

MOFs are hybrid crystalline materials composed of metal nodes connected by coordinating ligands.[18] Their versatility has generated significant interest in various fields, including adsorption, separation, catalysis, and sensing. This interest stems from the ability to fine-tune their properties by selecting specific metals,[19–21] modifying ligand structures,[22,23] and introducing functional groups[24–26] to meet the demands of particular applications.[27,28] ZIF-8 (zeolitic imidazolate framework),[29] a type of MOF, has attracted considerable interest due to its exceptional properties. Constructed from zinc cations linked by 2-methylimidazolate ligands, ZIF-8 stands out for its thermal and chemical stability,[30] ease of synthesis, and microporous structure. Its pore aperture of 3.4 Å and cavity size of 10 Å make it highly effective for molecular sieving and storage applications.[31–33]

To enhance the selectivity of chemiresistive sensors, ZIF-8 is often studied as a molecular sieving membrane that covers a sensitive ZnO layer. The ZnO layer serves a dual function: acting as a reservoir for Zn^{2+} ions and enabling *in situ* formation of the MOF. Various methods to convert ZnO into ZIF-8 have been reported, including mechanochemistry,[34] sonochemistry,[35] and solution-based chemistry,[36] each offering unique advantages in efficiency and scalability. The direct conversion of ZnO layers deposited by atomic layer deposition (ALD),[37] chemical vapor deposition (CVD)[36] or sputtering[37] onto various supports (*e.g.* alumina,[38] silicon,[39] PAN,..[40]) has been widely studied over the past decade. This research has also been extended to form advanced composites, such as 3D ZIF-8/CNT structures, with enhanced adsorption properties.[41] This method is also applied to coat ZnO-based chemiresistive sensors with various morphologies,[42] such as nanorods, nanofibers, tetrapods or supported thin films. Among various selective membrane approaches, ZIF-8 offers distinct advantages for improving gas-sensing applications thanks to its molecular sieving properties. Previous studies by our research group have demonstrated that ZIF-8 layers significantly enhance the selectivity of ZnO@ZIF-8 nanowire-based sensors.[43] The presence of ZIF-8 (pore aperture of 3.4 Å), can effectively separate H_2 from larger molecules like benzene and toluene, resulting in virtually zero gas sensing response to these larger molecules due to the size exclusion effect. Furthermore, Weber *et al.*[44] demonstrated further improvement of selectivity for H_2 over toluene, acetone, ethanol, and benzene using Pd-loaded ZIF-8 membranes on ZnO nanowire sensors showing high stability up to 300 °C during repetitive temperature cycling. Their results show that the addition of the ZIF-8 membrane layer achieved >1000% improvement in selectivity by completely eliminating sensor response to all interfering gases (toluene, acetone, ethanol, and benzene), while maintaining strong sensitivity to H_2, effectively transforming a multi-gas responsive sensor into one exclusively selective for hydrogen.

Overall, the molecular sieving strategy significantly improves selectivity of metal oxide sensors compared to conventional approaches, such as catalyst loading in metal oxides, which show less efficient molecular discrimination.[45,46] It also surpasses many other selective materials used directly as sensors like metal oxides or dense polymers, which often rely on other non-sieving mechanisms such as catalytic effects or differences in solution/diffusion rates.[47]

ZnO surfaces or films can be converted to ZIF-8 through two main methods: reaction with vaporized 2-methylimidazole[48,49] or direct solution-based conversion.[50] The solution-based approach is often preferred because it provides better control over ZIF-8 formation and allows ligand recycling (up to 50 times).[51] It involves five stages: ZnO dissolution, Zn^{2+} ion release and diffusion, ZIF-8 nucleation, crystal growth, and Ostwald ripening. Imbalances in these steps can lead to defects or incomplete formation of the ZIF-8 layer. Factors such as temperature,[52] ZnO deposition method,[37] crystallinity, crystal orientation,[53] solvent type,[52] and reagent ratio[54] critically influence the quality of ZIF-8 membranes.

While existing research offers valuable insights into optimizing the ZnO-to-ZIF-8 conversion process, several critical gaps remain. Specifically, the influence of solvent physicochemical properties - such as polarity, viscosity, and surface tension - has not been thoroughly investigated, leaving an incomplete understanding in this area. Additionally, studies on ZnO doping with other trivalent cations, such as aluminum have shown that solubility limits significantly affect material properties.[55] These findings suggest that similar effects may occur in Ga-doped systems.

Furthermore, the importance of achieving controlled and partial consumption of the ZnO layer, which is essential for preserving its electrical properties and sensitivity during ZIF-8 membrane formation, has often been overlooked. In addition, the role of annealing treatments of ZnO : Ga, commonly applied to enhance sensor performance, has not been adequately studied as a factor impacting the conversion process. Lastly, although doping is widely recognized for significantly enhancing the sensitivity and functionality of sensors, most studies focus solely on pristine ZnO, providing limited information on the behavior of doped ZnO systems during the conversion to ZIF-8. Hence, addressing these gaps is crucial for advancing the development of high-performance, selective sensors.

To tackle this issue, the present study aims to identify the critical factors affecting the controlled conversion of a high-performance ZnO : Ga layer into a uniform ZIF-8 membrane while preserving the ZnO : Ga layer to maintain its low electrical conductivity. Specifically, we have examined how solvent properties - such as polarity, surface tension, and viscosity-influence the ZnO-to-ZIF-8 conversion process. Additionally, we have explored the role of ZnO : Ga annealing in determining the uniformity and of the resulting synthetized ZIF-8 membrane. This work thus provides

valuable insights into optimizing the surface conversion of ZnO : Ga to ZIF-8, which will be applied in our future works to improve the selectivity of ZnO : Ga-based gas sensing layers.

Experimental section

Materials and methods

All reagents were purchased from commercial suppliers and used as received, without any additional purification. The entire synthesis process, from ZnO deposition to ZIF-8 formation, is illustrated in ESI† (Fig. S23).

Preparation of Si/SiO_2 substrates

Standard 4-inch n-type silicon wafers (engineering wafers) were selected as substrates for the deposition and characterization of gallium-doped zinc oxide (ZnO : Ga) thin films. Before deposition, the silicon wafers underwent a cleaning process involving immersion in buffered HF to remove native oxidation. They were then rinsed with deionized water and dried using a nitrogen gun to ensure a pristine, contaminant-free surface. To provide electrical insulation between the ZnO layer and the Si substrate, a 600 nm SiO_2 layer was deposited using the plasma enhanced chemical vapor deposition (PECVD) technique, matching the configuration of future sensor on microhotplate.

Deposition of ZnO : Ga thin films

Gallium-doped zinc oxide (ZnO : Ga) thin films were fabricated using physical vapor deposition (PVD) with an ALCATEL CIT SCM400 system operating in diode mode. The apparatus included a radio-frequency (RF) generator with a maximum power of 600 W for cathode polarization. The vacuum system, consisting of a primary pump and a secondary turbomolecular pump, achieved a base pressure of 10^{-5} Pa. The setup also featured a cooled target holder and two workstations equipped with a substrate cooling mechanism, ensuring precise control of the deposition parameters and film quality. Before deposition, the target underwent a 30-minute pre-sputtering process in an argon atmosphere containing 1% oxygen. This step was crucial for preventing target reduction during the subsequent deposition stages carried out in a pure argon environment. ZnO : Ga thin films were deposited under a working pressure of 1.8×10^{-2} mbar using RF power set to 30 W. The doping level, determined by CAMECA SXFiveFE electron probe microanalyser (EPMA) measurements, reached 4 at% of Ga, resulting in oxide films with the composition $Zn_{0.96}Ga_{0.04}O$. The film thickness, measured using a DEKTAK 3030 ST profilometer (VEECO), was around 50 nm with an uncertainty margin of ±10%. It should be noted that while Ga doping significantly enhances the electrical properties of ZnO for sensing applications, it does not notably affect the conversion process to ZIF-8. The small amount of Ga^{3+} cannot effectively coordinate with the imidazolate ligands to form stable MOF structures, thus having negligible impact on the dissolution-recrystallization mechanisms governing the conversion process.

Annealing of ZnO : Ga films

Annealed ZnO : Ga thin films were prepared by subjecting the as-deposited films to a controlled thermal treatment to ensure their stability for subsequent processes and measurement conditions. The films were placed in a furnace and heated to 600 °C for 4 hours in an air atmosphere. After annealing, the films were gradually cooled to room temperature inside the furnace to prevent thermal shock and maintain their structural integrity.

Conversion of ZnO-to-ZIF-8

The conversion of ZnO : Ga thin films into ZIF-8 was carried out using a (hydro)solvothermal treatment. The supported ZnO : Ga films were placed in a Teflon-lined stainless steel autoclave with a 45 mL capacity. This autoclave was filled with a 1% w/v solution of 2-methylimidazole (99%, Sigma Aldrich) dissolved in selected pure solvents or solvent mixtures, including DMF (99.8%), ethanol (absolute), and methanol (>99.8%) from Sigma Aldrich. The autoclave was then sealed and heated in a conventional oven at either 100 °C or 200 °C for durations ranging from 1.5 up to 12 hours, depending on the experimental protocol. After the conversion, the films were washed three times with methanol to remove any unreacted reagents and then dried in an oven at 70 °C for 2 hours.

Characterization of supported films

The structure and purity of the prepared films were analyzed using various analytical techniques, including X-Ray Diffraction (XRD), Fourier-transform infrared (FTIR) spectroscopy, field emission scanning electron microscopy (FESEM), and energy-dispersive X-ray spectroscopy (EDS). XRD patterns were recorded using a Bruker D8 Advance diffractometer equipped with a LynxEye detector. Measurements were performed using CuKα radiation (λ (CuKα_1) = 1.5405 Å). The diffractometer was configured in Bragg–Brentano geometry with an offset of 2° on θ, and data was collected with a step size of 0.02° in the 2θ range and a counting time of 1 second per step. Infrared spectra were obtained in the range of 600–2000 cm^{-1} with a resolution of 4 cm^{-1} using a Nicolet Nexus FT-IR in transmission mode.

A Ga-Focused Ion Beam (FIB)-FESEM dual beam FEI Helios NanoLab600i apparatus, equipped with an Oxford Instruments Aztec Advanced EDS system featuring an X-Max 80 mm^2 detector, was used for surface characterization and the preparation and analysis of film cross-sections. This system enabled high-resolution imaging and semi-quantitative chemical analysis of the thin films in both surface and cross-section views. To prevent damage to the samples during Ga-FIB milling, a platinum layer was deposited on the film surface. For surface imaging, a carbon layer was deposited to enhance conductivity and improve

Table 1 Values of dielectric constant, dipole moment, dynamic viscosity and interfacial tension for a series of studied solvents

Solvent	Dielectric constant (F m^{-1})	Dipole moment (D)	Dynamic viscosity at 20 °C (mPa s)	Interfacial tension (mN m^{-1})
MeOH	33.0	1.70	0.588	22.6
EtOH	25.3	1.69	1.095	22.3
DMF	36.7	3.82	0.92	36.4
H_2O	78.4	1.86	0.354	72.6

image clarity. Due to Ga milling, the analysis of Ga traces is not feasible on the cross-sections.

Results and discussion

Controlling the conversion of ZnO : Ga to ZIF-8 is essential for achieving a selective and sensitive membrane (permselectivity). This study investigates two main factors: the conversion rate and the quality of the resulting ZIF-8 membrane on the ZnO : Ga layer surface. To identify optimal interfacial process conditions, encompassing ZnO : Ga dissolution and ZIF-8 crystallization, a systematic analysis was performed on numerous samples prepared under different reaction conditions. The key parameters studied include: (i) solvent physicochemical properties, (ii) the MeOH/H_2O volumetric ratio, and (iii) annealing of the ZnO : Ga layer. The findings are discussed in the following sections.

Effect of solvent physicochemical properties on ZnO : Ga conversion to ZIF-8

The choice of solvent significantly influences the formation of a continuous ZIF-8 membrane. A series of solvents with varying physicochemical characteristics (Table 1) were selected for ZnO : Ga conversion under constant experimental conditions: ligand concentration (1 wt%), solvent volume (30 mL), reaction time (12 h), and temperature (100 °C). This enabled an exploration of the effects of key solvent parameters such as polarity, dynamic viscosity, and interfacial tension.

Structural analysis

XRD patterns of the converted samples demonstrate the strong influence of solvent properties on the conversion rate and crystallinity of ZIF-8 (Fig. 1a). Notably, when water is used as the solvent, both ZnO and ZIF-8 peaks are absent, indicating complete removal of the ZnO layer under hydrothermal conditions, a finding confirmed by IR spectroscopy (Fig. 1b). Despite the high dielectric constant of water (78.4), which should theoretically favor the deprotonation of the 2-mim ligand and promote the formation of ZIF-8, it instead promotes the protonation of the ligand by autoprotolysis of water. This process inhibits ZIF crystallization by favoring the reaction of Zn^{2+} cations with OH^- ions generated in solution, leading to the formation of zinc hydroxides. As a result, Zn^{2+} cations preferentially interact with water rather than with the ligand.

Besides solvent effects, the passivation of grain boundaries is crucial in determining the final structure quality. This has been demonstrated in other systems where ZIF-8-based composites effectively passivate boundaries in perovskite photodetectors.[56] For other solvents, ZnO undergoes partial conversion to ZIF-8, with different degrees of crystallinity. From the XRD patterns and IR spectra, the influence of the solvent on the conversion rate and ZIF-8 crystallinity,

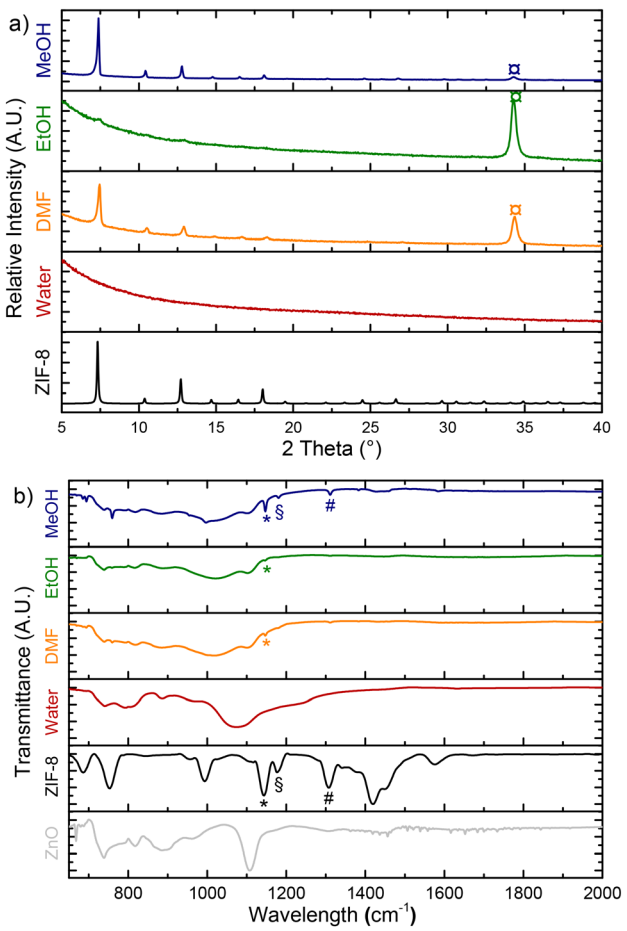

Fig. 1 a) XRD patterns of ZnO : Ga samples reacted/converted in different solvents (methanol, ethanol, DMF and water) at 100 °C for 12 h, compared with the theoretical pattern of ZIF-8. Major diffraction peaks are indexed with their corresponding Miller indices: ZIF-8 peaks at 2θ = 7.3° (011), 10.4° (002), 12.7° (112), 14.7° (022), 16.4° (013), 18.0° (222), 22.1° (114), 24.5° (233), 26.7° (134), and 29.6° (044); ZnO peaks at 2θ = 31.7° (100), 34.4° (002), and 36.2° (101) as indicated by (¤); b) Corresponding FTIR spectra, with (*) H_{ring} wag, (§) ring breathing (C–N symmetric stretch), and (#) H_{methyl} scissor, characteristic absorption bands of ZIF-8.

reflected by tighter and more intense XRD peaks, follows this order: EtOH < DMF < MeOH. This trend can be attributed to the differences in polarity, viscosity, and interfacial tension of the solvents.

Application of ethanol leads to the lowest crystallinity among the solvents tested, mainly due to its relatively low polarity when compared to DMF. Indeed, polarity plays a critical role in dissolving ionic compounds and facilitating the nucleation process necessary for ZIF-8 formation. Due to its lower polarity, ethanol struggles to effectively deprotonate the 2-mim ligand, a crucial step in the generation of ZIF-8 nuclei. This limitation results in fewer nuclei forming, thereby reducing the overall crystallinity. Additionally, its higher viscosity hampers the diffusion of reactants, leading to their less frequent mutual collisions, thereby impeding crystal growth. The resulting ZIF-8 crystals are smaller in size and poorly defined. Moreover, the higher interfacial tension of ethanol compared to DMF imposes a significant surface barrier to crystallization, which further suppresses nucleation and limits crystal growth.

In contrast, DMF demonstrates better performance due to its higher polarity and lower viscosity. Its superior polarity enhances the deprotonation of the 2-mim ligand, promoting a higher level of nucleation. The lower viscosity of DMF allows for more rapid diffusion of reactants, increasing their frequency of collisions and thus accelerating crystal growth. However, despite these advantages, the interfacial tension and nucleation dynamics associated with DMF are less effective to achieve high crystallinity compared to methanol.

In fact, methanol appears as the most effective solvent for promoting high crystallinity in ZIF-8. The combination of its high polarity and low viscosity creates an optimal environment for efficient nucleation and robust crystal growth. Its high polarity ensures advanced deprotonation of the 2-mim ligand, resulting in the formation of abundant nuclei. Simultaneously, its low viscosity facilitates rapid diffusion of reactants, enabling frequent interactions that support sustained crystal growth. These synergistic properties of methanol produce larger, well-defined ZIF-8 crystals with the highest degree of crystallinity obtained among the solvents tested.

Morphological analysis

SEM micrographs (Fig. 2) offer valuable insights that complement the findings from XRD and IR spectroscopy, shedding light on how each solvent affects the conversion of ZnO : Ga layers on silicon wafers. These micrographs allow to

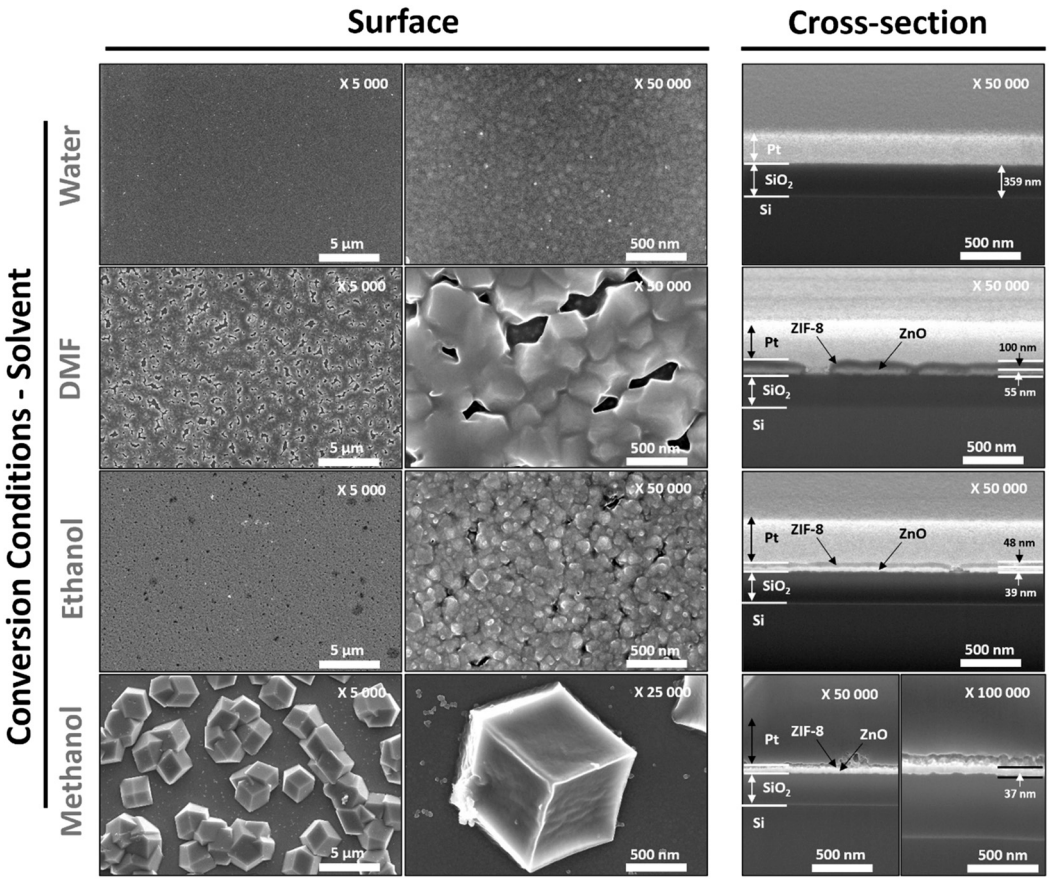

Fig. 2 SEM observations (surfaces and cross-sections) of ZnO : Ga samples after reaction/conversion at 100 °C for 12 h in various solvents (water, DMF, ethanol or methanol).

clearly evidence the presence, shape and size of ZIF-8 crystals while also revealing surface defects, which can compromise the membrane efficiency.

Water solvent. When water is used as a solvent for the conversion reaction, the ZnO : Ga layer is entirely dissolved and removed from the silicon wafer during hydrothermal treatment (Fig. 2). This is in line with the absence of ZnO-related XRD peaks in Fig. 1a. The surface observed in Fig. 2 corresponds to the pristine silica coating (Fig. S1†). This is also confirmed by the EDX analysis (Fig. S2†). In contrast, ZIF-8 crystals are visibly formed when other solvents are used. The size of these crystals increases when using solvents in the following order: EtOH < DMF < MeOH, consistent with the sharper and narrower XRD peaks observed previously.

DMF solvent. The surface morphology of samples converted on in DMF reveals compact clusters of fused ZIF-8 crystals (Fig. 2). However, these clusters are unevenly distributed, resulting in intercrystalline defects spanning a few hundred nanometers. Cross-sectional SEM micrographs suggest that these defects originate from irregular dissolution and crystallization processes across the surface (Fig. 2). The resulting layer exhibits two distinct regions: i) intercrystalline voids caused by complete dissolution of ZnO : Ga, and ii) superimposed bilayers of ZnO : Ga and ZIF-8.

For the ZnO : Ga/ZIF-8 bilayer, the ZnO : Ga layer thickness remains constant at approximately 55 nm, while the ZIF-8 layer grows to around 100 nm, indicating the consumption of about 36 nm of ZnO : Ga during the transformation. The intercrystalline spaces, initially filled by the ZnO : Ga layer, appear to serve as reservoirs of metal ions, supplying Zn^{2+} for ZIF-8 formation in adjacent regions. This interpretation is supported by EDS spectra (Fig. S3 and S4†), which show that areas with intercrystalline defects have low zinc content compared to silicon and oxygen from the wafer. In contrast, neighboring regions exhibit higher concentrations of zinc, carbon, and nitrogen, consistent with contributions from the ZIF ligand.

Ethanol solvent. Using ethanol as the solvent for ZnO : Ga conversion results in a relatively compact surface composed of small ZIF-8 crystals. While the surface quality improves compared to that obtained with DMF, SEM images reveal the presence of pinhole-type defects measuring hundreds of nanometers (Fig. 2). These defects, distinct from the intercrystalline defects observed with DMF, suggest that the conversion mechanism varies depending on the solvent.

Cross-sectional SEM micrographs show a well-defined ZnO/ZIF-8 stack (Fig. 2). The ZnO : Ga layer thickness decreases to about 39 nm, while the ZIF-8 layer grows to approximately 48 nm, consistent with the partial consumption of ZnO : Ga during conversion. In some areas, only ZIF-8 is observed, as confirmed by EDS analysis (Fig. S5 and S6†), indicating that pinholes may result from the complete local conversion of ZnO : Ga into ZIF-8.

However, these observations raise additional questions. Theoretical calculations reported elsewhere[57] predict that the ZIF-8 layer should be thicker than the original ZnO : Ga layer after complete conversion (an expansion factor up to 17 was calculated for ZIF-8, corresponding to the ratio of metal ion densities in the crystalline structure of the oxide and the MOF). Yet, in the pinhole regions, the layer thickness remains around 50 nm, comparable to the original ZnO : Ga layer. This anomaly suggests that in these regions a complete conversion releases excess Zn^{2+} ions into the surrounding medium. These ions may accumulate at the interface, potentially driving additional ZIF-8 formation near the pinholes.

Methanol solvent. The methanol-based conversion process, evidenced by sharp and intense XRD peaks and supported by SEM micrographs (Fig. 2) and EDS analysis (Fig. S7–S9†), produces highly crystalline, twinning micrometer-sized ZIF-8 crystals evidencing intergrowth process. In contrast to the spherical ZIF-8 nanoparticles (~100 nm) typically observed in the literature, the larger crystal size obtained in the present study underlines the role of interfacial species diffusion and concentration. This process is significantly influenced by the physicochemical properties of methanol and the specific chemical environment created during ZnO : Ga conversion, which diverges from conventional solution-state synthesis.

The ZIF-8 crystals formed during methanol conversion display specific morphological features, notably their faceted geometry. SEM micrographs reveal that most crystals adopt a rhombic dodecahedral shape with 12 exposed {110} facets (Fig. 2). According to the well-established crystallography of ZIF-8,[53,58] these facets correspond to {110} planes. This highly crystalline morphology is attributed to the slow growth rate of {110} facets,[59] which, according to Wulff's rule, determines the final crystal structure. A small fraction of the crystals exhibits a truncated cubic shape, typically associated with slower growth of {100} facets relative to {110}. This shape is often induced by capping agents like surfactants, and its presence, even in small quantities, suggests that during the conversion process, the growth of {100} facets might be selectively decelerated. While direct visualization of these crystallographic planes would require advanced techniques such as HR-TEM, the observed external morphologies align with the crystallographic features of ZIF-8 reported in the literature.[53,58,60]

The formation of such large, faceted ZIF-8 crystals can be explained by the interfacial conversion mechanism. In the early stages, the release of Zn^{2+} ions from the ZnO : Ga layer enriches the interfacial medium, temporarily creating a low ligand-to-metal molar ratio and a supersaturation regime. Similar conditions have been reported in the literature, where EDS spectroscopy showed elevated zinc concentrations on substrate surfaces outside ZIF-8 domains, peaking at 5.3% after three hours and declining gradually as Zn^{2+} is fully consumed after ten hours.[61]

This supersaturation regime enables two potential growth pathways. Both begin with the nucleation of crystalline primary particles (CPP), followed by growth through successive addition of either monomers (metal ions and ligands)[62] or secondary building units (SBUs).[63] These pathways contribute to the formation of the well-faceted crystals observed in SEM

micrographs (Fig. 2). As the Zn^{2+} concentration diminishes over time, crystal intergrowth becomes more prominent, transitioning from monomer- or SBU-driven growth to processes like polynuclear growth, internal reorganization, and aggregative growth. These mechanisms further enhance the observed crystal morphology.[64]

The results indicate that among the solvents studied, methanol is the most effective for promoting ZIF-8 crystallization, while water primarily facilitates ZnO : Ga dissolution. This highlights the dual importance of solvent selection in determining both the dissolution and crystallization dynamics of the conversion process. Other polar aprotic solvents with low viscosity, such as acetonitrile (dielectric constant: 37.5, dynamic viscosity: 0.369 mPa s, interfacial tension: 29.3 mN m^{-1}) and acetone (dielectric constant: 20.7, dynamic viscosity: 0.306 mPa s, interfacial tension: 23.7 mN m^{-1}), may exhibit intermediate behavior in this conversion process. The high polarity and very low viscosity of acetonitrile could potentially accelerate ZIF-8 nucleation while maintaining moderate dissolution rates, possibly resulting in smaller, and more numerous crystals with higher overall crystallinity compared to DMF. Conversely, acetone, with its lower polarity but similarly low viscosity, might favor controlled ZnO dissolution while promoting moderate crystal growth rates, potentially leading to a more uniform particle size distribution. Based on the trends observed in this study, these solvents could offer additional pathways for fine-tuning ZnO conversion kinetics. Future investigations should consider these solvents to expand the toolkit for ZIF-8 membrane engineering with tailored morphological properties.

Effect of MeOH/H_2O ratio on ZnO : Ga conversion to ZIF-8

The above studies using single solvents suggest that a solvent mixture might attractively combine their benefits while reducing inherent limitations. The solvent should be safe, eco-friendly, and ideally used under mild conditions with low temperatures and short processing times. Since the ZnO : Ga layer sensitivity depends on its thickness, minimizing Zn^{2+} depletion is crucial. Optimizing reaction conditions should also eliminate intercrystalline defects and pinholes to maintain the ZnO : Ga layer performance.

As discussed previously, DMF exhibits notable potential in ZIF-8 synthesis but is unsuitable due to health and environmental risks. Ethanol forms high-quality layers but has limited impact on oxide dissolution and MOF crystallization process. Water effectively dissolves the ZnO : Ga layer, providing Zn^{2+} ions for ZIF-8 formation, while methanol aids in crystallization, forming large, well-faceted ZIF-8 crystals. Both water and methanol influence ZnO : Ga dissolution and ZIF-8 formation, though neither component on its own can achieve the desired balance for optimal layer performance.

A water–methanol mixture was thus proposed to combine the strengths of both solvents while reducing their limitations. By adjusting methanol-to-water ratio, the process was optimized to enhance Zn^{2+} ion release or promote ZIF-8 crystallization. The conversion was optimized by maintaining a temperature of 100 °C, while reducing the reaction time from 12 hours to 1.5 hours. Three methanol-to-water ratios (1 : 3, 1 : 1, and 3 : 1) were tested, along with pure methanol for comparison. The structural and morphological characteristics of the corresponding samples synthetized in water–methanol solvent mixtures are reported and discussed in the following sections.

Structural analysis

The XRD patterns of the converted samples highlight the high degree of tunability and control achievable in the process (Fig. 3a). When the solvent mixture contains a higher

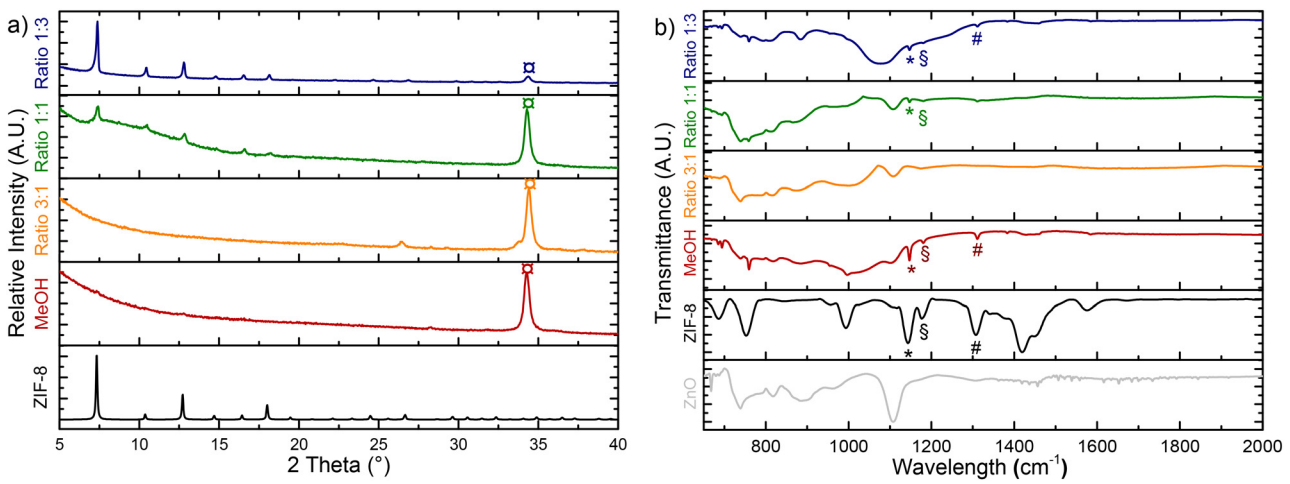

Fig. 3 a) XRD patterns of ZnO : Ga samples reacted/converted at 100 °C for 1.5 h in different CH_3OH/H_2O mixtures (ratios 1 : 3, 1 : 1 and 3 : 1), compared with the theoretical pattern of ZIF-8. (¤) indicates ZnO diffraction peak; b) corresponding FTIR spectra, with (*) H_{ring} wag, (§) ring breathing (C–N symmetric stretch), and (#) H_{methyl} scissor, characteristic absorption bands of ZIF-8.

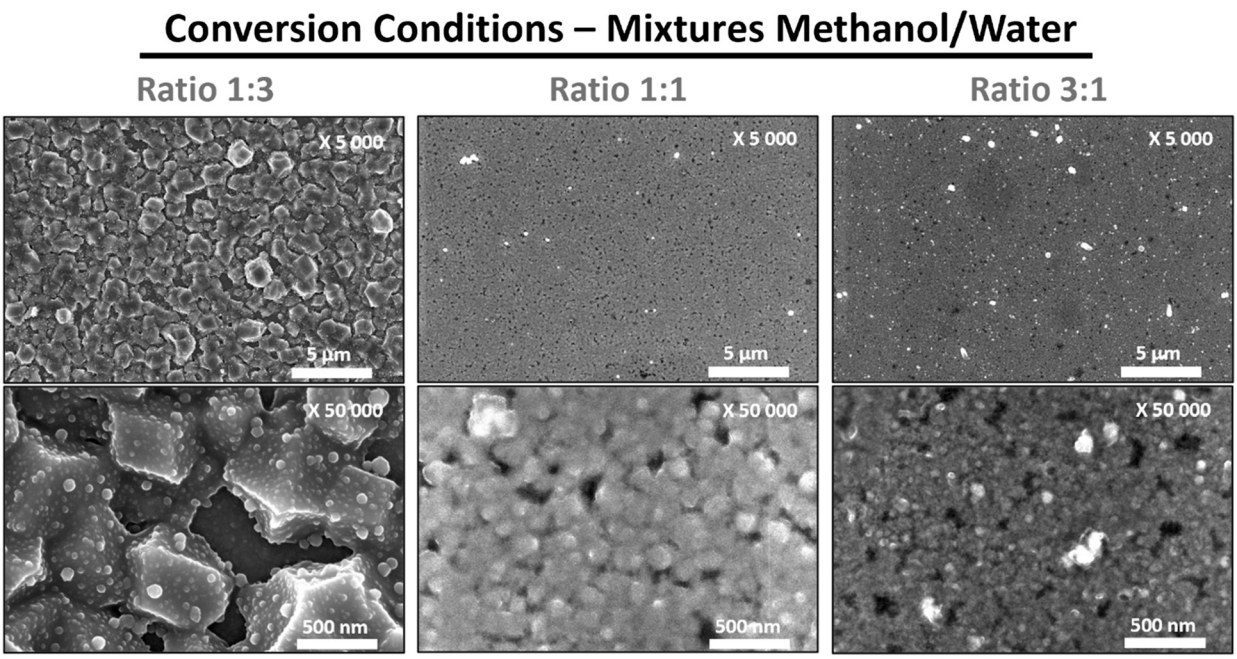

Fig. 4 SEM observations (surfaces) of ZnO : Ga samples after reaction/conversion at 100 °C for 1.5 h in CH_3OH/H_2O solvent mixtures with different ratios (1 : 3; 1 : 1 and 3 : 1).

proportion of water (CH_3OH/H_2O ratio: 1 : 3), the XRD peaks corresponding to ZIF-8 display higher intensity and sharpness than for the other samples. In addition, a significant reduction in the intensity of the ZnO : Ga XRD peaks indicates higher ZnO consumption and more advanced conversion.

As the water content in the solvent mixture decreases in favor of methanol, the intensity of the ZIF-8 XRD peaks weakens, and the peaks become broader, while the relative intensity of the ZnO : Ga peaks increases. Such result indicates a slower conversion rate and smaller ZIF-8 crystal sizes obtained in methanol solution with reduced water content. The infrared spectra (Fig. 3b) further confirm these observations, demonstrating that the $MeOH/H_2O$ solvent ratio can effectively regulate the conversion process. This allows for a precise control over the conversion rates, ranging from minimal to advanced, depending on the target reaction outcome.

Morphological analysis

SEM micrographs (Fig. 4 and 5) confirm an enhanced quality of the formed ZIF-8 layers and reveal clear trends. Adjusting the solvent ratio enables a fine control over crucial properties such as homogeneity, crystal size, defect reduction, and conversion rate, thus demonstrating the flexibility and effectiveness of this approach in optimizing the reaction process.

Methanol/water mixture (1 : 3). Using a water-enriched solvent mixture ($MeOH/H_2O$ ratio = 1 : 3) offers valuable insights into the conversion process by significantly enhancing ZnO : Ga dissolution. The higher water content facilitates ligand deprotonation due to its greater polarity, while its elevated surface tension reduces the likelihood of reactant collisions, delaying nucleation. Simultaneously, the lower viscosity improves diffusion, favoring crystal growth. These combined effects promote the formation of large ZIF-8 crystals, as evidenced by SEM micrographs and confirmed by EDS analysis (Fig. S10–S12†), which reveal micrometer-sized ZIF-8 crystals covering the surface of ZnO layers. However, such large crystals create intercrystalline defects at their boundaries (Fig. 4).

The ZIF-8 crystals feature an imperfect rhombic dodecahedral shape, coated with smaller spherical nanoparticles. This diminished crystal quality, compared to those formed in pure methanol, is attributed to faster dissolution kinetics and change in the physicochemical conditions at the crystal interface. Typically, a supersaturated environment with high Zn^{2+} concentration at the interface promotes the growth of well-defined, faceted crystals. However, in this scenario, the reduced viscosity allows Zn^{2+} ions to diffuse away from the interface more rapidly, disrupting the sustained high cation concentrations necessary for prolonged and precise crystal growth.

Two potential mechanisms could explain these observations:

1) Sequential growth and diffusion mechanism: water facilitates the rapid release of Zn^{2+} ions, creating a localized environment at the interface that favors the nucleation of crystalline primary particles (CPPs). These particles subsequently grow through the addition of monomers or secondary building units (SBUs). However, due to the low viscosity of water, Zn^{2+} ions quickly diffuse away from the interface, depleting the interfacial concentration. Such depletion prompts the formation of crystals *via* CPP

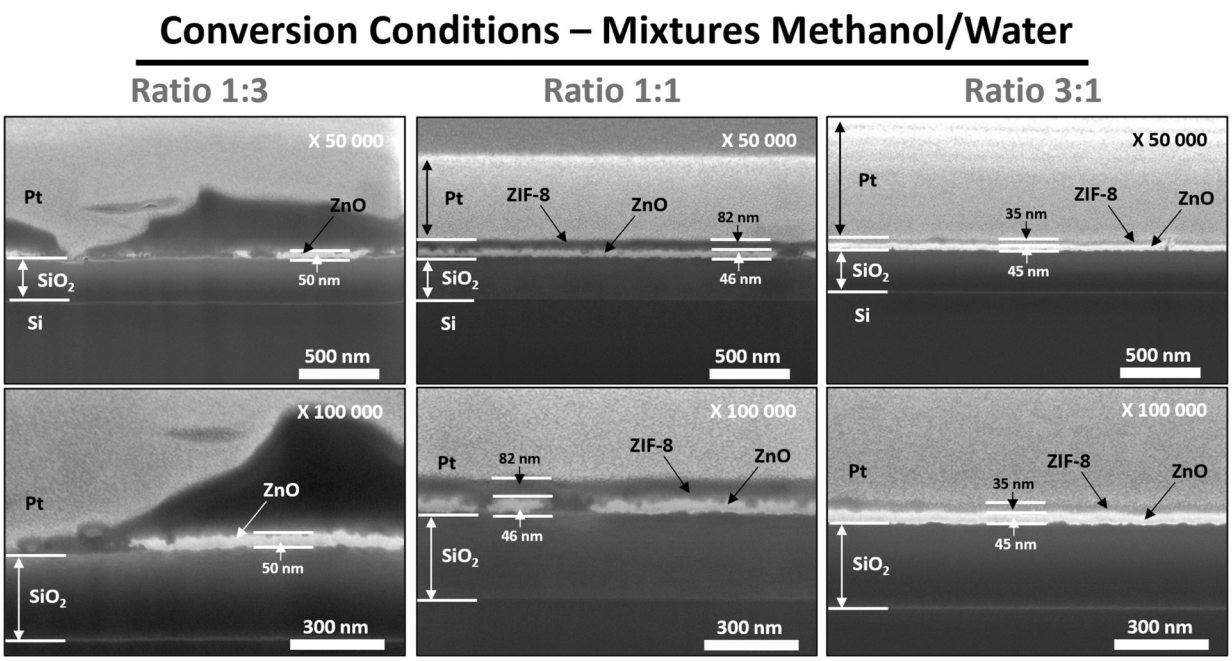

Fig. 5 SEM observations (cross-sections) of ZnO : Ga samples after reaction/conversion at 100 °C for 1.5 h in CH_3OH/H_2O solvent mixtures with different ratios (1 : 3; 1 : 1 and 3 : 1).

nucleation in a metastable phase, followed by polynuclear growth, resulting in smaller particles with irregular crystal shapes.

2) Growth, erosion, and secondary nucleation mechanism: initially, the rapid release of Zn^{2+} ions supports the growth of large, well-defined rhombic dodecahedral crystals. However, the strong erosive properties of water accelerate Zn^{2+} depletion, partially dissolving the ZIF-8 crystals through hydrolysis of zinc-nitrogen bonds. This process releases Zn^{2+} ions near the larger crystals, triggering secondary nucleation and forming smaller spherical nanoparticles. This secondary nucleation compromises the morphological integrity of the larger crystals.

The latter hypothesis is supported by reports of ZIF-8 undergoing cycles of growth and dissolution under similar conditions.[61] However, in the present study, these processes occur within 1.5 hours, hence significantly faster than the 10 hours reported elsewhere.[61] Such accelerated kinetics is likely due to the high water content, which enhances the hydrolysis of zinc–ligand bonds and speeds up dissolution.

Cross-sectional micrographs (Fig. 5) reveal the advanced dissolution of the ZnO : Ga layer caused by the high water content in the solvent mixture. Two distinct surface regions are evidenced: one where the ZnO : Ga layer has been completely replaced by a ZIF-8 layer, and another where the ZnO : Ga layer remains intact at its original thickness. Additionally, the resulting ZIF-8 layer exhibits significant surface irregularities. These observations suggest that excessive ZnO : Ga dissolution compromises sample quality, highlighting the need to reduce the water proportion in the solvent mixture.

Methanol/water mixture (1 : 1). SEM micrographs (Fig. 4) and EDS analysis (Fig. S13 and S14) confirm that the conversion in the presence of reaction mixture with lower water quantity ($MeOH/H_2O$ ratio = 1 : 1) leads to significantly better ZIF-8 layer quality. Indeed, the reduction in water content decreases ZIF-8 crystal size from micrometers to a few hundred nanometers. This effect arises from increased solvent viscosity, which slows crystal growth, and reduced interfacial tension facilitating the formation of a higher number of nuclei. Additionally, the solution enrichment in methanol affects the crystal morphology, yielding exclusively spherical particles instead of faceted crystals. Such observation suggests that slower ZnO : Ga dissolution lowers the Zn^{2+} concentration at the interface, promoting less defined morphologies. Crucially, the reduced water content minimizes intercrystalline defects, enhancing membrane quality.

Cross-sectional SEM micrographs (Fig. 5) reveal uniform conversion across the sample surface. The remaining ZnO : Ga layer retains a consistent thickness, indicating its controlled dissolution. However, isolated ZIF-8 regions are still observed on the surface, separated from the bilayer areas. These regions could affect system performance by increasing overall resistivity.

Methanol/water mixture (3 : 1). The $MeOH/H_2O$ (3 : 1) mixture was used to study the conversion process under conditions intended to slow ZnO : Ga dissolution while promoting ZIF-8 crystallization. SEM micrographs and EDS analysis (Fig. S15 and S16†) show that these conditions significantly improve surface homogeneity and compactness, aligning with trends observed for other solvent ratios (Fig. 4). The combination of increased viscosity and lower interfacial tension promotes the formation of smaller, more numerous crystals typically below 100 nm in size, hence significantly

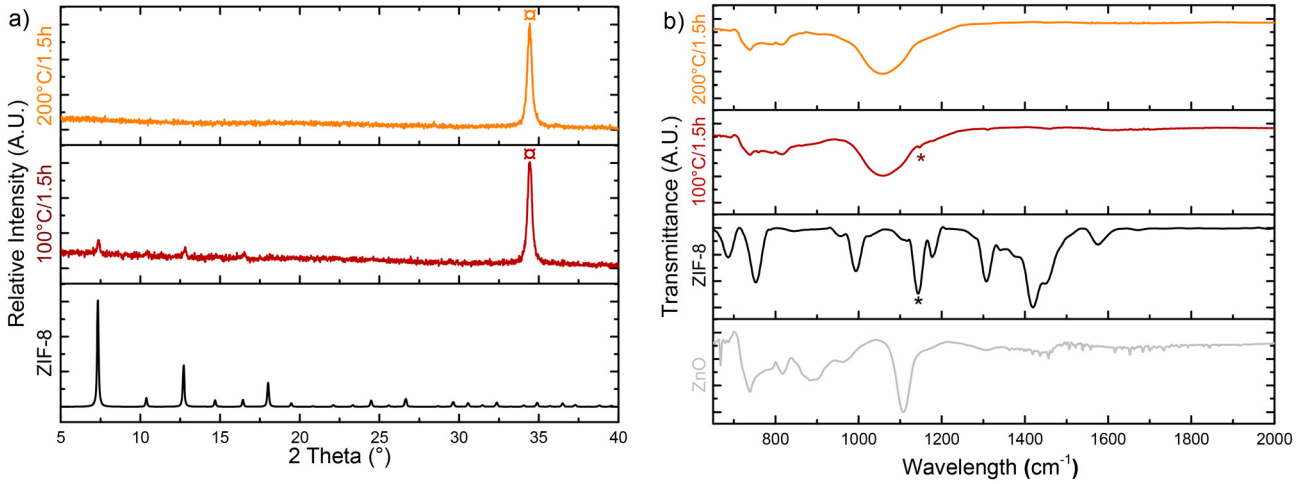

Fig. 6 a) XRD patterns of annealed ZnO : Ga samples reacted/converted in a CH_3OH/H_2O mixture (3 : 1) at 100 °C or 200 °C for 1.5 h, compared with the theoretical pattern of ZIF-8. (¤) indicates ZnO diffraction peak; b) corresponding FTIR spectra, with (#) H_{ring} wag vibrational band, characteristic of ZIF-8.

smaller than those formed in higher water content reaction mixtures. Additionally, reduced water content decreases surface defects resulting in enhanced ZIF-8 membrane quality.

Cross-sectional SEM micrographs (Fig. 5) confirm these improvements. The ZnO : Ga layer retains a constant thickness along the sample, similar to what was observed with the 1 : 1 solvent mixture. The lower water content significantly minimizes ZnO : Ga consumption during the conversion process. Importantly, the bilayer remains defect-free and continuous. Such optimized conditions allow for precise control of the ZnO : Ga dissolution rate, promoting effective ZIF-8 crystallization. This results in a high-quality bilayer system and a compact ZIF-8 membrane layer with only a slight reduction in ZnO : Ga thickness.

Interestingly, while a high water content in solvent mixtures adversely affects membrane formation, the presence of a small amount of water is crucial for achieving optimal membrane quality. This observation is supported by SEM micrographs of samples converted in pure methanol under the same reaction conditions (Fig. S17 and S18†), which reveal suboptimal results in the absence of water.

Impact of the annealing treatment of ZnO : Ga on its conversion to ZIF-8

Annealing temperature plays a crucial role in reaching the optimal sensitivity of metal oxides used in chemisensors, making thermal the treatment a common approach to enhance their sensing performance.[12] To examine the impact of annealing temperature on ZnO : Ga conversion, previously optimized conversion conditions were applied to ZnO : Ga films deposited on silicon wafers and annealed at 600 °C for 4 hours. Furthermore, the effect of more extreme conversion conditions was evaluated by increasing the conversion temperature from 100 °C to 200 °C.

Structural analysis

The analysis of the recorded XRD patterns reveals significant differences compared to non-annealed ZnO : Ga samples converted under similar conditions, highlighting the pronounced impact of the thermal treatment (Fig. 6a). The XRD patterns of the annealed sample converted at 100 °C for 1.5 h show peaks corresponding to the ZIF-8 structure, with higher intensity than those of the non-annealed sample, thus indicating better ZIF-8 formation on the surface. These peaks are broad, suggesting the presence of ZIF-8 nanodomains. However, the remaining ZnO : Ga is still significantly present. Interestingly, increasing the conversion temperature from 100 °C to 200 °C (for 1.5 h) results in no detectable XRD peaks corresponding to the ZIF-8 structure in the resulting sample. These findings are consistent with the recorded IR spectra (Fig. 6b).

Morphological analysis

Conversion at 100 °C for 1.5 h. The SEM micrographs support the findings from the XRD analysis. The surface of the annealed sample, converted at 100 °C for 1.5 h, shows the ZIF-8 islands with undefined shapes surrounded by grain boundary defects (Fig. 7). In contrast, the non-annealed sample has a more homogeneous and continuous surface with fewer defects and very small spherical nanoparticles (Fig. 4 and 5). The larger ZIF-8 crystal size observed in the annealed sample is likely due to changes in ZnO : Ga reactivity induced by the annealing treatment. Studies have shown that ZnO annealed at 600 °C dissolves more quickly in water due to an increased number of oxygen vacancies on the surface and within the bulk of the metal oxide.[65,66]

When ZnO is annealed at 600 °C, several structural changes occur at the atomic level. The thermal energy causes oxygen atoms to migrate to the surface, where they can desorb as O_2, creating oxygen vacancies within the metal

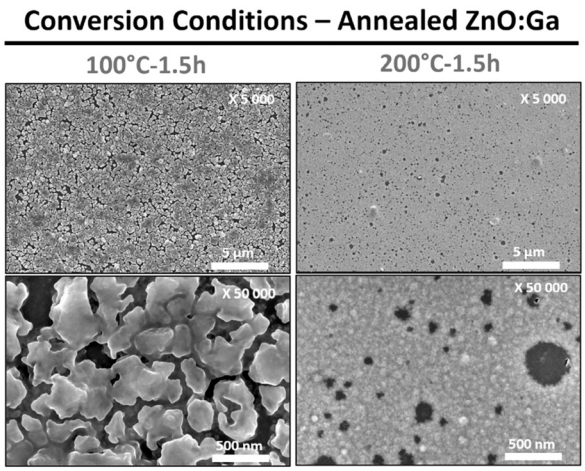

Fig. 7 SEM observations (surfaces) of annealed ZnO : Ga samples after reaction/conversion in a CH_3OH/H_2O mixture (3 : 1) at different temperatures (100 °C and 200 °C) for 1.5 h.

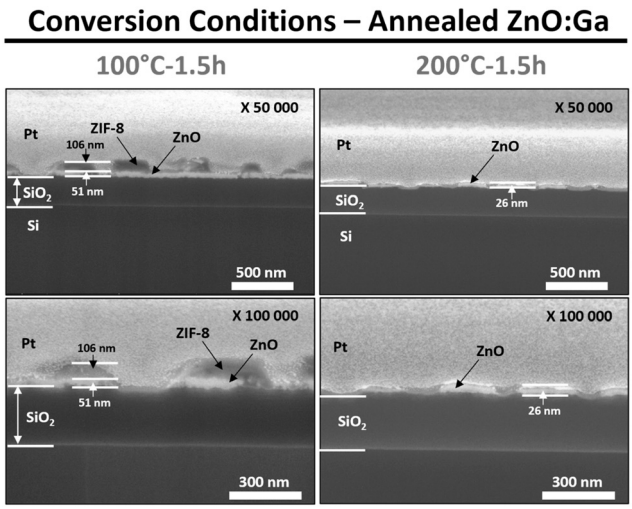

Fig. 8 SEM observations (cross-sections) of annealed ZnO : Ga samples after reaction/conversion in a CH_3OH/H_2O mixture (3 : 1) at different reaction temperatures (100 °C and 200 °C) for 1.5h.

oxide lattice.[65] These vacancies generate localized regions of positive charge (defects) due to the missing O^{2-} ions. During the subsequent conversion process, these defects serve as preferential dissolution sites, allowing water molecules to more readily weaken the Zn–O bonds and facilitate the release of Zn^{2+} ions into the solution. Additionally, the increased surface energy at defect sites promotes faster chemical reactions.

The higher concentration of Zn^{2+} ions at the interface then promotes the formation of larger ZIF-8 crystals. This finding is not surprising as for smaller ZIF-8 particles higher molar ratios of 2-methylimidazole to zinc ions is typically required. It should be mentioned that excessive 2-methylimidazole can coat ZIF-8 surfaces and slow the growth of crystal nuclei, but this effect is less significant in this case. The defects observed in the annealed sample are therefore caused by the accelerated ZnO : Ga dissolution, which hinders the uniform crystallization of ZIF-8 at the interface.

Cross-sectional micrographs show that the regions with ZIF-8 islands consist of a bilayer of ZnO : Ga and ZIF-8, while the grain boundary defects reveal the absence of matter, exposing the silicon wafer below (Fig. 8). This indicates that the Zn^{2+} ions necessary for ZIF-8 crystallization are initially supplied by the ZnO : Ga surrounding the islands.

Conversion at 200 °C for 1.5 h. For the annealed sample converted at a higher temperature (200 °C), XRD analysis does not show any ZIF-8 signatures. SEM micrographs reveal a granulated surface with pinholes hundreds of nanometers in size (Fig. 7). These findings indicate that the annealed ZnO : Ga dissolves more rapidly, and the increased conversion temperature accelerates the dissolution rate, thereby hindering the crystallization of ZIF-8 at the metal oxide interface.

Cross-sectional micrographs provide further evidence for this hypothesis (Fig. 8). The images reveal a single layer of residual ZnO : Ga surrounded by voids, exposing the silicon wafer to the environment. This confirms that under such reaction conditions, ZnO : Ga dissolution dominates over ZIF-8 crystallization, resulting in an incomplete conversion process.

These findings highlight the critical role of thermal treatment in influencing the dissolution kinetics of ZnO : Ga. They emphasize the importance of adjusting conversion conditions to slow down dissolution while enhancing ZIF-8 crystallization, ensuring a balanced dissolution/crystallization process and its effective control. The quality parameters of the ZIF-8 membranes optimized in this study should directly impact their molecular sieving performance in gas sensing applications, as demonstrated in our previous works.[43,44] Furthermore, the literature extensively documents how ZIF-8 membrane characteristics influence sensing selectivity and response.[16] The controlled membrane thickness (~50–100 nm) achieved in our study represents an optimal balance between selectivity and response kinetics. Literature indicates that thicker ZIF-8 membranes (>200 nm) typically result in lower selectivity, preventing even H_2 molecules from passing through.[67] Conversely, an insufficient conversion rate may lead to cracks in the membrane or incomplete coverage, compromising selectivity.

The high crystallinity of the ZIF-8 layer optimized in this work, evidenced by sharp XRD peaks (Fig. 3a), ensures consistent 3.4 Å pore apertures across the membrane. This aperture size is ideal for selectively allowing H_2 (kinetic diameter: 2.9 Å) to pass while blocking larger molecules such as acetone (4.6 Å), ethanol (4.5 Å), and benzene (5.9 Å).[68] Finally, the proposed controlled conversion process preserves a significant portion of the underlying ZnO layer, which is critical for maintaining electrical conductivity for the sensing mechanism. The membrane quality parameters achieved in this study, particularly defect density, crystallinity, and thickness control, align well with those identified in the

literature as determinants of superior molecular sieving performance.

This investigation thus demonstrates that solvent properties play a crucial role in ZIF-8 membrane engineering, while the characteristics of the metal oxide layer significantly influence the dissolution mechanism and, consequently, membrane quality. Our optimized synthesis conditions (3 : 1 MeOH/H_2O ratio, 100 °C, 1.5 hours) provide precise control over ZnO dissolution and promote effective ZIF-8 crystallization. This results in a high-quality, uniform bilayer system with consistent thickness across the substrate and nanoscale crystals forming a compact layer, potentially suitable as a selective membrane barrier in chemiresistive sensor applications. Further examination of the metal oxide surface chemistry, which depends notably on deposition conditions and thermal treatment, is essential for a complete mechanistic understanding. These findings lay the groundwork for developing precise conversion protocols to engineer selective chemiresistive sensors, which will be further refined by additional studies of metal oxide chemistry. Our experimental approach has provided mechanistic insights through systematic investigation of solvent effects and thermal treatments. Recent advanced studies in the literature further support our mechanistic interpretations. Tao *et al.* investigated the interplay between organic linkers and ZnO substrates during ZIF-8 crystallization using *in situ* atomic force microscopy combined with *ab initio* molecular dynamics and density functional theory calculations. Their work revealed that organic ligands selectively bind to ZnO surface steps, controlling dissolution kinetics and thereby regulating MOF overgrowth.[53] This selective binding mechanism aligns with our observations of how different solvents influence ZnO dissolution rates. Additionally, Sinnwell *et al.* utilized *in situ* X-ray diffraction to reveal the time-resolved formation of ZIF-8 and intermediary ZnO@ZIF-8 composites, demonstrating temperature-dependent mechanisms throughout the reaction process.[69,70] These findings parallel our observations regarding the critical role of temperature in balancing dissolution and crystallization kinetics.

While our study focuses on optimizing practical conversion conditions through systematic experimental investigation, these advanced mechanistic studies provide complementary theoretical foundations that support the proposed conversion mechanisms and the observed effects of solvent properties and ZnO thermal treatment on ZIF-8 growth.

Conclusions

This study systematically explores the liquid-phase conversion of ZnO : Ga to ZIF-8, examining the influence of the solvent physicochemical properties, solvent mixtures, reaction time and temperature including thermal treatment conditions of the metal oxide layers. It highlights key factors affecting the conversion process and provides valuable strategies for tuning chemiresistive sensor features, offering more versatility compared to vapor-phase conversions, which are limited by fewer variables.

The results emphasize the importance of solvent physicochemical properties, such as polarity, viscosity, and interfacial tension, in controlling the ZnO : Ga conversion rate and ZIF-8 crystallinity. Methanol, while effectively dissolving, excels in promoting ZIF-8 crystallization. Attractively, by utilizing methanol–water mixtures, the dissolution and crystallization processes can be precisely regulated and optimal balanced. For example, a 3 : 1 CH_3OH/H_2O ratio minimizes defects formation and ensures a thin, uniform bilayer structure, making it ideal for the preparation of continuous ZIF-8 layers on ZnO : Ga thin films.

The effect of annealing on ZnO : Ga conversion underscores the critical role of controlling dissolution kinetics. Annealing has been shown to enhance the reactivity of ZnO : Ga by increasing oxygen vacancies, which accelerates dissolution, and influences MOF crystal growth. However, higher temperatures can lead to excessive dissolution, hindering ZIF-8 crystallization and compromising the structural integrity of the ZIF-8 layer.

This study highlights the importance of optimizing solvent compositions, conversion parameters, and metal oxide thermal treatments to produce defect-free ZIF-8 membrane layers. In a broader context, these findings offer valuable insights for improving fabrication techniques in chemiresistive sensors, targeting superior sensitivity, selectivity, and environmental sustainability for practical applications. These insights are crucial for optimizing ZIF-8 selective films on metal oxide thin layers, paving the way for developing highly selective gas sensors based on sensitive semiconductors like ZnO. Our future research will focus on implementing these optimized ZIF-8 membranes in functional gas sensors based on ZnO semiconductor thin films and evaluating their selectivity enhancement in real-world conditions for specific target gases. Building on our previous work with ZnO@ZIF-8 systems, sensors fabricated using optimized conversion protocols are expected to demonstrate enhanced selectivity while maintaining high sensitivity.

Data availability

The data supporting this article have been included as part of the ESI.†

Author contributions

Conceptualization, methodology and validation: KD, BP, AJ, LP. Investigation: KD, BP, LP and MD; data curation: KD, LP. Writing – original draft preparation: KD. Writing – review and editing: KD, BP, DF, PM, MB, MD, LP, AB, and AJ. Supervision: MD, LP and AJ. Project administration & funding acquisition: LP, AJ, DF, PM. All authors have read and agreed to the published version of the manuscript.

Conflicts of interest

There are no conflicts to declare.

Acknowledgements

This work received funding from the French ANR agency under grant agreements ANR-20-CE04-0012 and ANR-23-CE42-0029. It was supported by the LAAS-CNRS micro and nanotechnologies platform, a member of the Renatech French national network. The authors thank Claudie Josse and Sophie Gouy from the Centre de Microcaractérisation Raimond Castaing (UAR 3623) for their support with FIB and EPMA characterizations.

Notes and references

1 A. Kushwaha, R. Kumar and N. Goel, *FlatChem*, 2024, **43**, 100584.
2 N. Ramgir, N. Datta, M. Kaur, S. Kailasaganapathi, A. K. Debnath, D. K. Aswal and S. K. Gupta, *Colloids Surf., A*, 2013, **439**, 101–116.
3 P. Recum and T. Hirsch, *Nanoscale Adv.*, 2024, **6**, 11–31.
4 S. K. Singh, D. Dutta, S. Das, A. Dhar and M. C. Paul, *Mater. Sci. Semicond. Process.*, 2020, **107**, 104819.
5 A. Dey, *Mater. Sci. Eng., B*, 2018, **229**, 206–217.
6 M. A. Franco, P. P. Conti, R. S. Andre and D. S. Correa, *Sens. Actuators Rep.*, 2022, **4**, 100100.
7 P. M. Bulemo, *ACS Appl. Electron. Mater.*, 2023, **5**, 2106–2114.
8 G. Paul and S. Sen, *Mater. Lett.*, 2002, **57**, 742–746.
9 R. Wang, A. W. Sleight and D. Cleary, *Chem. Mater.*, 1996, **8**, 433–439.
10 M. Lalanne, J. M. Soon, A. Barnabé, L. Presmanes, I. Pasquet and P. Tailhades, *J. Mater. Res.*, 2010, **25**, 2407–2414.
11 J. L. Noel, R. Udayabhaskar, B. Renganathan, S. Muthu Mariappan, D. Sastikumar and B. Karthikeyan, *Spectrochim. Acta, Part A*, 2014, **132**, 634–638.
12 B. Paret, R. Monflier, P. Menini, T. Camps, Y. Thimont, A. Barnabé and L. Presmanes, *Chemosensors*, 2024, **13**, 1.
13 E. B. Kim, K. Y. Shin, W. Oum, S. Moon, A. Mirzaei, S. S. Kim and H. W. Kim, *Sens. Actuators, B*, 2025, **426**, 137021.
14 M. Weber, J.-Y. Kim, J.-H. Lee, J.-H. Kim, I. Iatsunskyi, E. Coy, P. Miele, M. Bechelany and S. S. Kim, *J. Mater. Chem. A*, 2019, **7**, 8107–8116.
15 M. Lesego, D. T. Ndinteh, P. Ndungu and M. A. Mamo, *Heliyon*, 2023, **9**, e22329.
16 T. Shi, S. Hussain, C. Ge, G. Liu, M. Wang and G. Qiao, *Rev. Chem. Eng.*, 2023, **39**, 911–939.
17 G. Zhang and Y. Wang, *Polyoxometalates*, 2023, **2**, 9140020.
18 W. Lu, Z. Wei, Z. Y. Gu, T. F. Liu, J. Park, J. Park, J. Tian, M. Zhang, Q. Zhang, T. Gentle, M. Bosch and H. C. Zhou, *Chem. Soc. Rev.*, 2014, **43**, 5561–5593.
19 K. A. Forrest, T. Pham, S. K. Elsaidi, M. H. Mohamed, P. K. Thallapally, M. J. Zaworotko and B. Space, *Cryst. Growth Des.*, 2019, **19**, 3732–3743.
20 K. Dedecker, M. Drobek, V. Rouessac and A. Julbe, *ACS Appl. Mater. Interfaces*, 2023, **15**, 6831–6838.
21 B. Van De Voorde, M. Hezinová, J. Lannoeye, A. Vandekerkhove, B. Marszalek, B. Gil, I. Beurroies, P. Nachtigall and D. De Vos, *Phys. Chem. Chem. Phys.*, 2015, **17**, 10759–10766.
22 N. M. Padial, E. Quartapelle Procopio, C. Montoro, E. López, J. E. Oltra, V. Colombo, A. Maspero, N. Masciocchi, S. Galli, I. Senkovska, S. Kaskel, E. Barea and J. A. R. Navarro, *Angew. Chem., Int. Ed.*, 2013, **52**, 8290–8294.
23 K. Dedecker, M. Drobek and A. Julbe, *J. Phys. Chem. B*, 2023, **127**, 11091–11099.
24 J. Pires, J. Fernandes, K. Dedecker, J. R. B. Gomes, G. Pérez-Sánchez, F. Nouar, C. Serre and M. L. Pinto, *ACS Appl. Mater. Interfaces*, 2019, **11**, 27410–27421.
25 K. Dedecker, R. S. Pillai, F. Nouar, J. Pires, N. Steunou, E. Dumas, G. Maurin, C. Serre and M. L. Pinto, *ACS Appl. Mater. Interfaces*, 2018, **10**, 13886–13894.
26 R. Banerjee, A. Phan, B. Wang, C. Knobler, H. Furukawa, M. O'Keeffe and O. M. Yaghi, *Science*, 2008, **319**, 939–943.
27 K. Dedecker, E. Dumas, B. Lavédrine, N. Steunou and C. Serre, *Metal-Organic Frameworks (MOFs) for Environmental Applications*, Elsevier, 2019, pp. 141–178.
28 S. Dasgupta, S. Biswas, K. Dedecker, E. Dumas, N. Menguy, B. Berini, B. Lavedrine, C. Serre, C. Boissière and N. Steunou, *ACS Appl. Mater. Interfaces*, 2023, **15**, 6069–6078.
29 A. Phan, C. J. Doonan, F. J. Uribe-Romo, C. B. Knobler, M. Okeeffe and O. M. Yaghi, *Acc. Chem. Res.*, 2010, **43**, 58–67.
30 K. S. Park, Z. Ni, A. P. Côté, J. Y. Choi, R. Huang, F. J. Uribe-Romo, H. K. Chae, M. O'Keeffe and O. M. Yaghi, *Proc. Natl. Acad. Sci. U. S. A.*, 2006, **103**, 10186–10191.
31 K. Dedecker, M. Drobek and A. Julbe, *Molecules*, 2024, **29**, 5825.
32 K. Dedecker, M. Drobek and A. Julbe, *RSC Appl. Interfaces*, 2025, **2**, 364–372.
33 T.-M. T. Nguyen, J.-W. Chen, M.-T. Pham, H. M. Bui, C.-C. Hu, S.-J. You and Y.-F. Wang, *Environ. Technol. Innovation*, 2023, **31**, 103169.
34 S. Tanaka, K. Kida, T. Nagaoka, T. Ota and Y. Miyake, *Chem. Commun.*, 2013, **49**, 7884–7886.
35 L. Bazzi, I. Ayouch, H. Tachallait and S. EL Hankari, *Results Eng.*, 2022, **13**, 100378.
36 Y. Yue, Z.-A. Qiao, X. Li, A. J. Binder, E. Formo, Z. Pan, C. Tian, Z. Bi and S. Dai, *Cryst. Growth Des.*, 2013, **13**, 1002–1005.
37 K. Khaletskaya, S. Turner, M. Tu, S. Wannapaiboon, A. Schneemann, R. Meyer, A. Ludwig, G. Van Tendeloo and R. A. Fischer, *Adv. Funct. Mater.*, 2014, **24**, 4804–4811.
38 J. Yu, Y. Pan, C. Wang and Z. Lai, *Chem. Eng. Sci.*, 2016, **141**, 119–124.
39 A. J. Cruz, I. Stassen, M. Krishtab, K. Marcoen, T. Stassin, S. Rodríguez-Hermida, J. Teyssandier, S. Pletincx, R. Verbeke, V. Rubio-Giménez, S. Tatay, C. Martí-Gastaldo, J. Meersschaut, P. M. Vereecken, S. De Feyter, T. Hauffman and R. Ameloot, *Chem. Mater.*, 2019, **31**, 9462–9471.
40 M. Bechelany, M. Drobek, C. Vallicari, A. Abou Chaaya, A. Julbe and P. Miele, *Nanoscale*, 2015, **7**, 5794–5802.
41 I. Dönges, M. I. Büschges, C. Njel and J. J. Schneider, *Dalton Trans.*, 2022, **51**, 13725–13733.
42 Z. L. Wang, *Mater. Today*, 2004, **7**, 26–33.

43 M. Drobek, J. H. Kim, M. Bechelany, C. Vallicari, A. Julbe and S. S. Kim, *ACS Appl. Mater. Interfaces*, 2016, **8**, 8323–8328.
44 M. Weber, J.-H. Kim, J.-H. Lee, J.-Y. Kim, I. Iatsunskyi, E. Coy, M. Drobek, A. Julbe, M. Bechelany and S. S. Kim, *ACS Appl. Mater. Interfaces*, 2018, **10**, 34765–34773.
45 A. S. Mokrushin, I. A. Nagornov, T. L. Simonenko, N. P. Simonenko, P. Y. Gorobtsov, T. V. Khamova, G. P. Kopitsa, A. N. Evzrezov, E. P. Simonenko, V. G. Sevastyanov and N. T. Kuznetsov, *Mater. Sci. Eng., B*, 2021, **271**, 115233.
46 J.-H. Kim, J.-H. Lee, Y. Park, J.-Y. Kim, A. Mirzaei, H. W. Kim and S. S. Kim, *Sens. Actuators, B*, 2019, **294**, 78–88.
47 G. Eranna, B. C. Joshi, D. P. Runthala and R. P. Gupta, *Crit. Rev. Solid State Mater. Sci.*, 2004, **29**, 111–188.
48 I. Stassen, N. Campagnol, J. Fransaer, P. Vereecken, D. De Vos and R. Ameloot, *CrystEngComm*, 2013, **15**, 9308.
49 J.-B. Lin, R.-B. Lin, X.-N. Cheng, J.-P. Zhang and X.-M. Chen, *Chem. Commun.*, 2011, **47**, 9185.
50 M. Drobek, M. Bechelany, C. Vallicari, A. Abou Chaaya, C. Charmette, C. Salvador-Levehang, P. Miele and A. Julbe, *J. Membr. Sci.*, 2015, **475**, 39–46.
51 Y. Li, C. Ma, P. Nian, H. Liu and X. Zhang, *J. Membr. Sci.*, 2019, **581**, 344–354.
52 Y. Wang, H. Zhang, X. Wang, C. Zou, B. Meng and X. Tan, *Ind. Eng. Chem. Res.*, 2019, **58**, 19511–19518.
53 J. Tao, M.-S. Lee, M. L. Sushko, J. J. De Yoreo, J. Liu, Z. Zhang, D. Banerjee, S. Akkineni, M. E. Bowden, P. K. Thallapally, Y. Shin and M. A. Sinnwell, *Chem. Mater.*, 2020, **32**, 6666–6675.
54 R. Freund, A. E. Lanza, S. Canossa, M. Gemmi, J. Goscianska, V. Cauda, M. Oschatz and S. Wuttke, *Chem. Mater.*, 2023, **35**, 1891–1900.
55 B. Mockenhaupt, J. K. Wied, S. Mangelsen, U. Schürmann, L. Kienle, J. Schmedt auf der Günne and M. Behrens, *Dalton Trans.*, 2023, **52**, 5321–5335.
56 S. Duan, X. Xu, W. Chen, J. Zhi and F. Li, *Polyoxometalates*, 2022, **1**, 9140003.
57 K. Khaletskaya, S. Turner, M. Tu, S. Wannapaiboon, A. Schneemann, R. Meyer, A. Ludwig, G. Van Tendeloo and R. A. Fischer, *Adv. Funct. Mater.*, 2014, **24**, 4804–4811.
58 J. Cravillon, S. Münzer, S.-J. Lohmeier, A. Feldhoff, K. Huber and M. Wiebcke, *Chem. Mater.*, 2009, **21**, 1410–1412.
59 Y. Pan, D. Heryadi, F. Zhou, L. Zhao, G. Lestari, H. Su and Z. Lai, *CrystEngComm*, 2011, **13**, 6937.
60 K. Kida, M. Okita, K. Fujita, S. Tanaka and Y. Miyake, *CrystEngComm*, 2013, **15**, 1794.
61 H. Yoo and N. Shin, *Appl. Surf. Sci.*, 2023, **625**, 157211.
62 P. Y. Moh, P. Cubillas, M. W. Anderson and M. P. Attfield, *J. Am. Chem. Soc.*, 2011, **133**, 13304–13307.
63 J. Cravillon, C. A. Schröder, R. Nayuk, J. Gummel, K. Huber and M. Wiebcke, *Angew. Chem., Int. Ed.*, 2011, **50**, 8067–8071.
64 J. A. Allegretto, D. Onna, S. A. Bilmes, O. Azzaroni and M. Rafti, *Chem. Mater.*, 2024, **36**, 5814–5825.
65 H. He, J. Cao, X. Fei and N. Duan, *Environ. Int.*, 2019, **130**, 104930.
66 H. He, J. Cao, X. Fei and N. Duan, *Sci. Total Environ.*, 2021, **787**, 147545.
67 R. Lv, Q. Zhang, W. Wang, Y. Lin and S. Zhang, *Sensors*, 2021, **21**, 4069.
68 T. Zhou, Y. Sang, X. Wang, C. Wu, D. Zeng and C. Xie, *Sens. Actuators, B*, 2018, **258**, 1099–1106.
69 B. Jin, S. Wang, D. Boglaienko, Z. Zhang, Q. Zhao, X. Ma, X. Zhang and J. J. De Yoreo, *J. Cryst. Growth*, 2023, **603**, 126989.
70 M. A. Sinnwell, Q. R. S. Miller, L. Liu, J. Tao, M. E. Bowden, L. Kovarik, D. Barpaga, Y. Han, R. Kishan Motkuri, M. L. Sushko, H. T. Schaef and P. K. Thallapally, *ChemSusChem*, 2020, **13**, 2602–2612.